IEEE Access
Multidisciplinary ⋮ Rapid Review ⋮ Open Access Journal

Received 19 June 2023, accepted 18 July 2023, date of publication 7 September 2023, date of current version 12 September 2023.

Digital Object Identifier 10.1109/ACCESS.2023.3308068

APPLIED RESEARCH

Phased Array Antenna System Enabled by Liquid Metal Phase Shifters

SHAKER ALKARAKI[1], (Member, IEEE), QUAN-WEI LIN[2], (Member, IEEE), JAMES R. KELLY[3], (Member, IEEE), ZHENGPENG WANG[4], (Member, IEEE), AND HANG WONG[2], (Senior Member, IEEE)

[1]Department of Electrical and Electronic Engineering, George Green Institute for Electromagnetics Research, University of Nottingham, NG7 2RD Nottingham, U.K.
[2]State Key Laboratory of Terahertz Millimeter Waves, Department of Electrical Engineering, City University of Hong Kong, Hong Kong
[3]Electronic Engineering and Computer Science, Queen Mary University of London, E1 4NS London, U.K.
[4]School of Electronics and Information Engineering, Beihang University, Beijing 100191, China

Corresponding author: Shaker Alkaraki (Shaker.Alkaraki@nottingham.ac.uk)

This work was supported by the Engineering and Physical Research Council under Grant EP/P008402/1, Grant EP/P008402/2, and Grant EP/V008420/1.

ABSTRACT This paper introduces a proof of concept design for the first phased array antenna design enabled by liquid metal (LM) technology. The proposed LM phased array antenna system is based on substrate integrated waveguides (SIW) to excite an 1×4 printed dipole antenna array. To effectively control the phase distribution on SIW power dividers, the liquid metals performed as a shorting pin along the body of the SIW are implemented. The proposed LM integrated SIW structure enables a large-phase tuning ratio of 360°. This new LM based phase shifters perform stable, low loss and wideband performance for the phased antenna array. In addition, a reconfigurability of the phase controls on the proposed phased antenna array can be realized when the LMs are filled in and out on the designated vias on the SIWs. To validate the proposed antenna array, simulation and measurement are carried out in this work. A prototype of the proposed LM phased array antenna operates at 10 GHz is measured, which confirms the array can have a 12% impedance bandwidth and the maximum gain of 8.3dBi with the scanning range of ±38° along the end-fire direction. This proposed technology is reliable and cost-effective for wideband phased array applications

INDEX TERMS Liquid metal, EGaIN, phased array, phase shifters, reconfigurable antenna, substrate integrated waveguide.

I. INTRODUCTION

There is strong interest in beam steerable antennas for applications such as: millimeter-wave mobile access for 5G communications, satellite internet, radar detection, etc.. These applications require high-gain beam steerable antennas to compensate for the path loss in wave propagation and enable mobility. The most popular techniques for steering a high-gain beam, include: 1) phased array antennas, 2) mechanical movement, 3) metamaterial, 4) mode switching, 5) element switching. The techniques have been listed in approximate order of popularity with item 1 being most popular and item 5 being least poplar. Let us briefly overview each technique. Phased array antennas [1], [2] are attractive because they enable electronically controlled beam steering in small angular steps. However, the approach relies on the use of a signal distribution network incorporating phase shifters and sometimes adjustable attenuators [1], [2]. This kind of signal distribution network adds to the complexity of designing the array together with the cost of fabrication. Additionally, analogue phased array antennas require phase shifters which tend to exhibit high insertion losses, especially at millimetre wave frequencies. There is interest, therefore in developing low loss phase shifting technology and that is the focus of this paper. Mechanical steering can enable continuous beam steering. This is typically achieved by moving the component on the

The associate editor coordinating the review of this manuscript and approving it for publication was Bilal Khawaja.

antenna body such as feed, reflector [3], lens [4], or metamaterial surface [5], [6], [7], [8]. The RF losses associated with mechanical steering are typically very low. However, mechanical moving parts are often undesirable because they require periodic maintenance, repair, and replacement. Metamaterial techniques are often deployed in conjunction with mechanical steering and where this is the case they require mechanical movement of a feed or metamaterial surface. On other occasions switches or varactors [9], [10] are used to tune the properties of the metasurface to steer or switch a beam. Mode switching involves altering the eigenmode of current supported within the radiating element of an antenna. In this way it is possible to switch the main beam direction. Typically, this is achieved by employing switching or tuning elements, within the radiating element, to alter the current path. Alternatively, it can be achieved by altering the location of the feed excitation point [11]. This would require the use of an SPxT switch (where x is an integer) within the feed network and the associated disadvantages of this are discussed in the following text. Element switching involves switching the feed excitation between a series of radiating elements each exhibiting a directional radiation pattern pointing towards a different direction [12], [13]. In this way it is possible to switch the beam direction. However, this involves using a SPxT switch where x is an integer representing the number of directional radiating elements. As x is increased so the losses, within the switch, increase.

Recently, antenna researchers demonstrated Ferroelectric Ceramics [14], [15], [16], Liquid crystal [17], [18], [19], and Micro-electromechanical systems (MEMS) [20] for phased antenna array design for low GHz to millimeter-wave applications. These approaches may produce a low-power consumed solution for the large active antenna arrays but the phase tunings are usually limited and the structures of these kinds of antenna arrays are complicated. Among most of the phase array designs, the employment of PIN diodes, GaAs FETs, CMOS are the most popular in designing phase shifters for the phased arrays Nevertheless, these technologies have several limitations. On one hand, PIN diodes phase shifters have high insertion losses [21] and phase shifters based on GaAs FETs have relatively lower IL than competing devices but have limited radio frequency (RF) power handling capability [22], [23]. On the other hand, phase shifters based on CMOS technology are small in size and have high resolution and accuracy but their main disadvantage is that of limited output powers and losses in amplitude with relatively poor noise figure because of high IL and nonlinearity [24], [25], [26]. For example, a typical IL performance for a state-of-the-art CMOS based active phase shifter is much higher than 10 dB at 10 GHz [24], [25], [26], [27].

Figure-of-merit (FoM) is a commonly utilized metric for the comparison of phase shifter performance [16], [17], [18], [19], and is given in (1).

$$FoM = \frac{\Delta \emptyset_{max}}{IL_{max}} \tag{1}$$

where, IL_{max} is the maximum insertion loss and $\emptyset_{max}$ is the ratio of maximum phase shift and at particular frequency.

The use of LM in for design of various microwave devices such as: antennas, filters, phase shifters and switches have been proved by prior works [28], [29], [30], [31], [32], [33], [34], [35], [36], [37], [38], [39], [40], [41], [42], [43], [44], [45], [46], [47], [48], [49], [50], [51], [52]; however, there was no demonstration for: 1) phase shifters achieve very high phase shift up to 360° and 2) for the phased antenna array by the integration of LM network. For instance, the phase shifter discussed in [32] attains a complete 180° phase shift, while achieving an FoM of 78.3 °/dB at a frequency of 10GHz. This phase shifter implementation utilizes the switched line technique, relying on an array of LM vias to facilitate switching between multiple SIW transmission lines, each with distinct electrical lengths. However, it is worth noting that this approach has its limitations. The maximum achievable phase shift is confined to 180°, and the operational bandwidth of the phase shifter is relatively narrow. Furthermore, phase shifters has notable physical size. The design complexity of the phase shifter outlined [32] stems from the substantial quantity of LM vias needed to redirect electromagnetic waves along various pathways. These characteristics prove to be disadvantages when considering the integration of such a phase shifter with other circuitry, such as the feeding structure associated with a phased array antenna.

In this paper, we introduce an innovative approach to develop a large phase tuning range technique for a phased antenna array. The approach of using liquid metals (LM), based on alloys of Gallium, to perform a control of the phase for a SIW-type power divider such that the beam forming from an 1×4 antenna array can be achieved. Our proposed phased array is designed based on liquid metal phase shifter that is the first LM based phase shifter having a tuning range of up to 360° together with a very low IL and a small electrical size. The phase shifter showcases an impressive FoM of 131.3 °/dB at 10GHz. This FoM is exceptionally high. Additionally, another significant benefit of the suggested phase shifter is its relatively compact total electrical length. This attribute enhances its suitability for integration within an SIW feeding network, facilitating the realization of a beam-scanning phased array.

In addition, the liquid in-and-out controls for the LM phase shifter can enable beam configurations for the phased antenna array. Also, we hypothesize that the proposed phased array will be able to handle very high RF power. This observation arises from the absence of factors within LM that could potentially constrain its capacity to handle RF power. Consequently, the RF power-handling capability of the SIW phased array will be solely bound by the inherent characteristics of the SIW transmission line. Our expectation is that the proposed phased array will deliver notably improved linearity performance [53]. Finally, the suggested LM phased array antenna stands as an excellent choice for applications

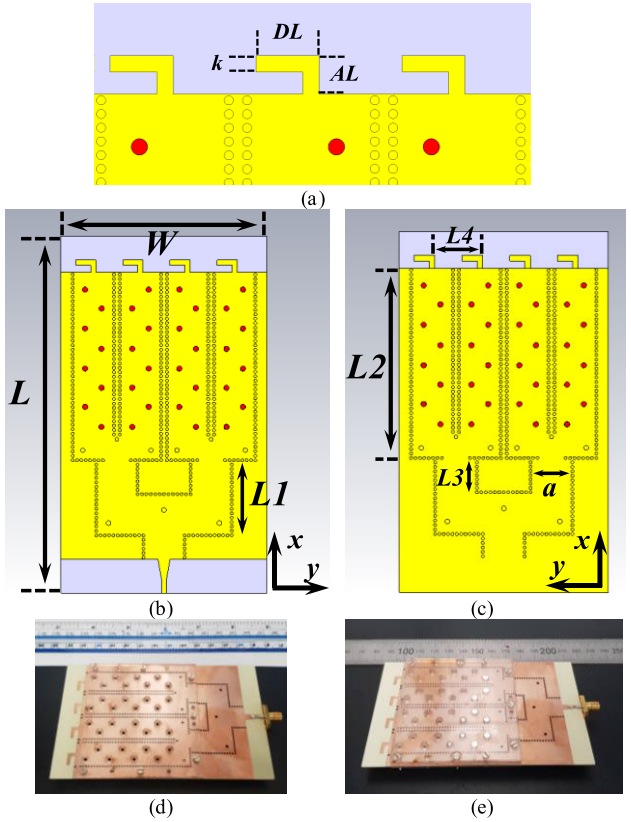

FIGURE 1. The schematic of the entire phased array antenna system enabled by LM technology. (a) Inset view of the printed dipole antenna, (b) top view of the entire phased array, (c) bottom view of the entire phased array. Key: substrate = light violet, copper = yellow, copper plated vias = yellow, liquid metal vias = red.

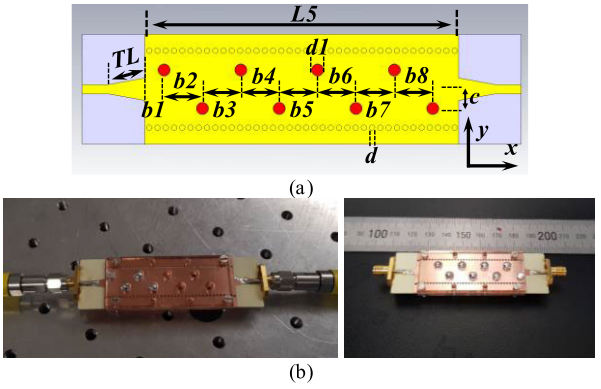

FIGURE 2. The schematic of the proposed LM phase shifter used within the phased array antenna. (a) Top view showing the dimensions, and (b) photographs of the prototype. Key: substrate = light violet, copper = yellow, copper plated vias = yellow, liquid metal vias = red.

demanding a combination of low loss performance and robust power handling capabilities.

II. STRUCTURE OF THE LIQUID METAL PHASED ARRAY AND PHASE SHIFTER

Fig. 1 shows the structure of the proposed LM phased array antenna along with the fabricated prototype. Fig. 2 shows the structure of an isolated LM phase shifter along with a fabricated prototype. Our first step was to design the phase shifter, shown in Fig. 2, in isolation. Its performance was then fully characterized and measured. Next four phase shifters were integrated within an SIW feeding structure to design the full phased array antenna, shown in Fig.1. Both the proposed phase shifter and phased array were designed to operate on a Rogers 4003C substrate. 4003C has a dielectric constant (ε_r) of 3.55, a loss tangent ($tan\delta$) of 0.0027, and a thickness (h) of 0.813mm. Four LM phase shifters, each incorporating eight LM vias were integrated within the SIW feeding structure. The length of the phased array antenna was (L) and the width is (W). The width of the SIW is a and the length of the first stage of the SIW power splitter is $L1$. The length of the second stage of the SIW feeding structure, which incorporates the phased shifters is ($L2$). The copper vias which are used within SIW have a diameter of d. In addition, an array of four identical printed dipole antennas was integrated within the phased array, as shown in Fig.1 (a-c). The separation distance between each of the four printed dipole is ($L4$) and the dimension of each printed dipole are as follows: dipole arm length (AL), dipole length (DL) and width of dipole (k). One SMA connector was used to feed the entire phased array antenna, as shown in Fig. 1 (d-e) and two SMA connectors are used to feed the isolated phase shifter as shown in Fig. 2. The SMA connectors are attached to the SIW by means of a short transition incorporating a tapered section of microstrip transmission line. The width of the transition is (TW) and the length of transition is (TL). Each phase shifter incorporates eight drill holes. Those drill holes can be filled with or emptied of liquid metal in order to alter the phase shift. Hence forth they will be referred to as LM vias or simply as vias. The maximum available phase shift, available from each phase shifter, is ∼360°. The LM vias have a diameter of $d1$.The distance between the edge of SIW and first LM via is ($b1$), while the distance between the first via and the second via is ($b2$). Similarly the distance between the second LM via and third LM via is ($b3$) and so on for the other vias. The distance between all of the LM vias and the center of the SIW, in the y-direction is c. Table 1 gives the dimensions of the proposed liquid metal phased array antenna and an isolated phase shifter.

TABLE 1. The dimension of the proposed phase array and phase shifter (UNIT: MM).

$a = 14$	$L = 121.1$	$W = 70$	$L1 = 22.5$
$L2 = 63$	$L3 = 11.5$	$L4 = 16$	$AL = 4.2$
$d = 1$	$d1 = 1.8$	$DL = 6.9$	$k = 1.8$
$c = 3$	$TL = 6.8$	$TW = 4.1$	$b1 = 2.6$
$b2 = 6.7$	$b3 = 5.7$	$b4 = 6.2$	$b5 = 6.1$
$b6 = 6$	$b7 = 6.3$	$b8 = 6.2$	

III. OPERATING PRINCIPLES AND RESULTS FOR THE ISOLATED PHASE SHIFTER

A. OPERATING PRINCIPLES

Established theory shows that a phase shift can be generated by a high pass filter when it is used as a switched

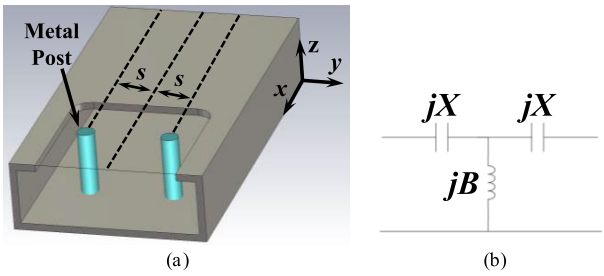

FIGURE 3. Rectangular waveguide with conductive posts. (a) Conductive posts incorporated in the waveguide, and (b) single post's equivalent circuit.

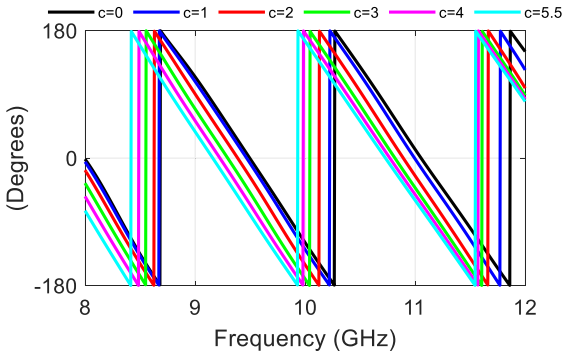

FIGURE 4. Impact of *c* on the phase of the proposed phase shifter at 10 GHz.

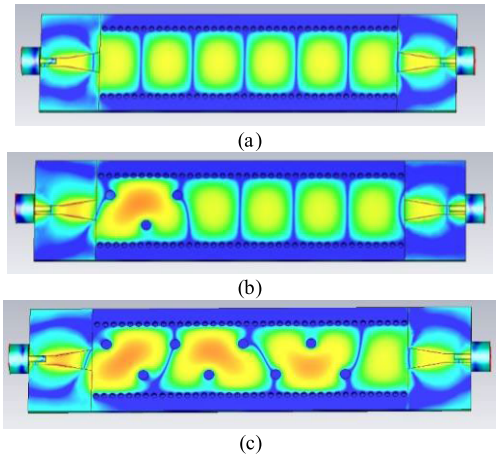

FIGURE 5. The distribution of electric field distribution within the proposed phase shifter, both in the presence and absence of LM vias. (a) No vias, (b) 3 vias and (c) 8 vias.

high-pass/low-pass topology [54], [55], [56], [57]. A specific configuration of a high-pass filter, extensively examined within rectangular waveguides [54], [58], [59] and involves the utilization of conductive posts as illustrated in Fig. 3. These conductive posts bear similarity to vias employed in SIW transmission lines. For isolated metal post, the phase shift is controlled by the post diameter and the horizontal position of the post s with respect to the E-plane wall of the waveguide. In addition, one post, can be represented by a lumped element equivalent circuit consisting of a T-network of components. Such a network behaves as a high-pass filter [54], [56], where the susceptance B and the reactance X control the phase shift (φ) as shown in (2):

$$\varphi = \frac{B + 2X - BX^2}{2(1 - 2BX)} \tag{2}$$

Indeed, the inclusion of one via within an SIW transmission line induces a phase shift, which correlates directly with the diameter ($d1$) of the via and inversely with the distance (c) separating the center of the SIW transmission line from the via's position along the y-axis orientation. An individual via causes an advance in the phase of the electromagnetic (EM) wave as it propagates inside the SIW transmission line, as depicted in Fig. 4. To be precise, incorporating the via reduces the electrical length of the SIW causing a shorter electrical path that inherently advances the phase of the EM wave. By incorporating more vias, the electrical length of the path is further reduced, as illustrated in Fig. 5. Consequently, this leads to an increased phase advance, which contributes to a greater degree of controllable phase shift. The magnitude of the phase shift can be controlled by varying the distance between the vias along the x-axis direction.

For a fixed via diameter, the phase shift and the insertion loss (IL) contributed by a single LM via can be controlled by the horizontal position of the via (c) as shown in Fig. 4. Specifically, the phase shift caused by a single via is inversely proportional to the value of c. For instance, when the via diameter is 2 mm, a range of phase shifts from 7.8° to 88.8° can be achieved in increments of approximately 1° by gradually varying c from 5.5 mm to 0 mm as shown in Fig. 4.

Moreover, by incorporating additional LM vias, the overall phase shift delivered by the phase shifter can be improved. The precise value of the phase shift and the corresponding IL can be controlled by adjusting the horizontal spacing between two LM vias along the x-axis direction ($b2$ to $b8$). This relationship is demonstrated in Fig. 6. For instance, adding any additional LM via after the first LM via yields a phase shift ranging from 22.5° to 58° per additional LM via, as shown in Fig. 6(a) which corresponds to IL within a range 1.65dB to 4.8dB, as shown in Fig. 6(b). Adding additional LM vias enables us, to design a reconfigurable phase shifter, incorporating eight LM via that can achieve a phase shift of up to 360°. The phase shifter can have 9 states with a step size of ∼45°, as summarized in TABLE. 2.

The dimensions of the SIW transmission line were determined using the design process outlined in [60], [61], and [62]. The width of the SIW transmission line (a) determines the cut-off frequencies of the TE_{10} and TE_{20} modes. In more detail, the TE_{10} and TE_{20} modes establish the lower and upper cut-off frequencies, respectively, for the SIW transmission line. In this particular case, the lower cut-off frequency was set at 5.7GHz, while the upper cut-off frequency was chosen as 11.6GHz. These cut-off frequencies were calculated using

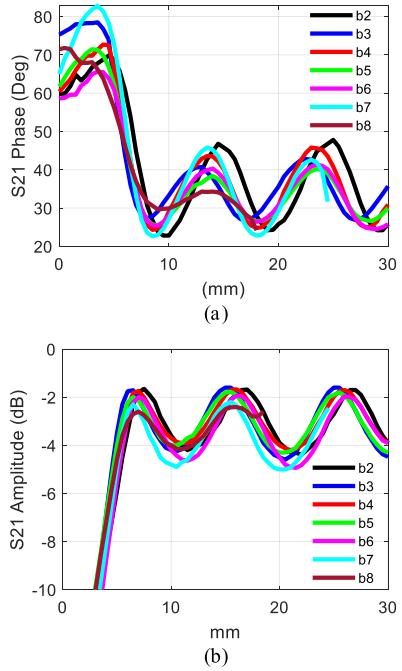

FIGURE 6. The S_{21} of the proposed phase shifter for different horizontal separation values between the LM vias. (c = 3 mm). (a) Phase and (b) amplitude.

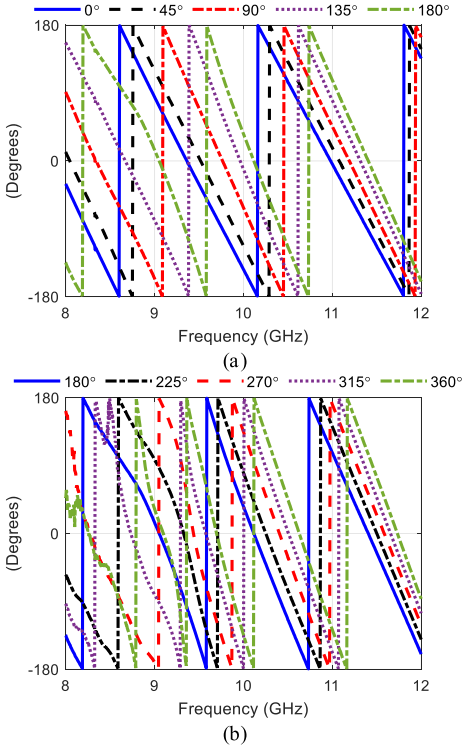

FIGURE 7. The measured S21 phase response for all operating states of the proposed phase shifter. (a) 0° to 180° and (b) 180° to 360°.

TABLE 2. Phase shifter scheme.

State	Number of Active LM Via	Total Phase shift
State 1 (S1)	0	0
State 2 (S2)	1	45°
State 3 (S3)	2	90°
State 4 (S4)	3	135°
State 5 (S5)	4	180°
State 6 (S6)	5	225°
State 7 (S7)	6	270°
State 8 (S8)	7	315°
State 9 (S9)	8	360°

equations (3) and (4).

$$F_{k,mn} = \frac{k}{2\sqrt{\varepsilon_r}}\sqrt{\left(\frac{m}{a}\right)^2 + \left(\frac{n}{h}\right)^2} \tag{3}$$

$$F_{C,m0} = \frac{mc}{2a\sqrt{\varepsilon_r}} \tag{4}$$

where: k is the light speed in vacuum, m and n are integers and h is the height of SIW.

Subsequently, a tapered transition was developed to facilitate the seamless transition from microstrip to SIW. A replicated version of this transition was incorporated on both sides of the SIW transmission line. To finalize the design, each of the microstrip lines were terminated with an SMA connector. The design guidelines provided in [61] and [63] were employed to ensure the proper design of the tapered transition. The optimization of the transition's length (TL) and width (TW) was carried out using the CST Microwave Studio®. Furthermore, the phase shift of the phase shifter was controlled through the incorporation of more LM vias. In essence, the design methodology of the proposed phase shifter can be succinctly outlined as follows:

A. To obtain the desired phase shift, the initial step is to introduce the first LM via and optimize its position along the y-axis (c). The position of $b1$ has no impact on the phase shift, as the phase shift is controlled with c. In the case of the proposed phase shifter, c was set at 3 mm to achieve a phase shift of 31°. This specific value was chosen to ensure that the IL remains below 2.4dB at 10GHz.

B. optimize the distance $b2$ to achieve a phase shift of ≈45° after the addition of the 2nd via.

C. The process described in step B is repeated for the remaining LM vias, from the third via to the eighth via, by optimizing the parameters $b3$ to $b8$. A phase shift value of approximately 47° was selected for these vias, ensuring that the phase shift achieved by all eight LM vias sums up to 360°.

B. EXPERIMENTAL RESULTS

The total phase shift achieved by the isolated phase shifter is up to 360°, with step of ∼45°. The achieved phase shift depends on the number of used LM vias. The measured and simulated S_{11}, S_{22}, and S_{21} performance of the proposed device are shown in Figs. 7 and 8. At 10 GHz, for all phase shifting states, the proposed phase shifter has an IL

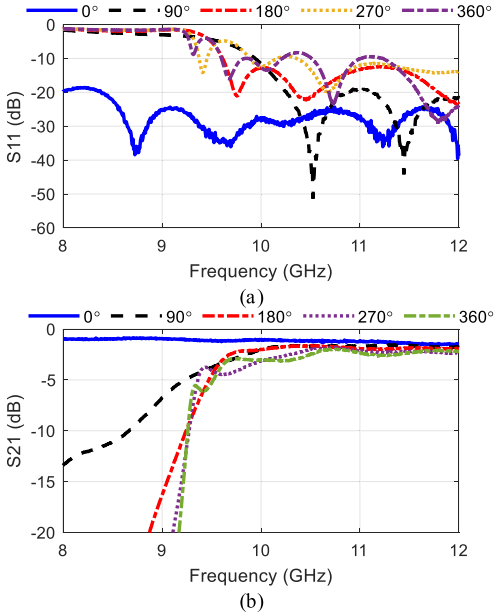

FIGURE 8. Measured S-parameters for the proposed phase shifter. (a) S11, and (b) S21.

lower than 2.8dB, as shown in Fig. 8 (b). In addition, in all operation states, the RMS amplitude error of the proposed phase shifter is below 1.5dB and the RMS phase error is less than 20° over wide bandwidth ranging between 9.6GHz and 11.5GHz. In the frequency range spanning approximately 9GHz to 9.25GHz, notable elevation in both *IL* and return loss (RL) values is evident, particularly in instances where the phase shift surpasses 180°. This phenomenon can be attributed to the inherent characteristics of the proposed phase shifter, which exhibit traits resembling those of high-pass filters. Furthermore, the phase shifter's behavior gives rise to the emergence of a quasi-filter effect, complete with a 3dB cut-off frequency. The specifics of this cut-off frequency, where signal power dwindles by half (-3dB), are contingent upon the phase shifter's operational state. Across all operational states, the 3dB cut-off frequency spans the interval from roughly 8GHz to around 9.5GHz. The simulated and measured phase results exhibit notable alignment. The proposed phase shifter achieves a cumulative measured phase shift of 368.6°, whereas simulation yields a phase shift of 360.5° when all LM vias are activated. The specifics of the phase and *IL* outcomes at 10GHz are succinctly presented in TABLE 3. Discrepancies between measured and simulated phase shifts are primarily ascribed to fabrication tolerances, particularly concerning the positioning and dimensions of each via hole. For instance, sensitivity analyses conducted in simulation reveal that a fabrication tolerance of 0.1 mm in the *c* value could introduce a phase shift alteration of up to 2.8°. Similarly, a 0.1 mm tolerance in the *b2* to *b8* dimensions might lead to a phase shift variance of up to 2.5°. Lastly, the *IL* of the phase shifter is mainly due to losses associated with matching and dissipation within the substrate. Table 4 provides a comprehensive comparison of the performance exhibited by the proposed liquid metal (LM) phase shifter in contrast to a range of cutting-edge LM phase shifters, alongside alternative technologies, all functioning at a frequency of 10 GHz. The proposed phase shifter has exceptional FoM of 131.3 °/dB which is higher than all other alternative phase shifters reported in [14], [15], [16], [17], [18], [19], [20], [21], [22], [23], [24], [25], [26], [32], and [51], and including digital phase shifters in [24], [25], [26], and [64]. Furthermore, the suggested liquid metal (LM) phase shifter exhibits very low insertion loss (IL) and minimal root mean square (RMS) amplitude variations, with values below 1.5dB for all states. Notably, the *IL* performance of the proposed phase shifter is better (i.e. lower) than all of state-of-the-art counterparts capable of providing a phase shift of up to 360°, demonstrating superior performance in terms of lower *IL*. In addition, the LM phase shifter is designed using SIW technology and is fed through SMA connectors. It is anticipated that the LM phase shifter possesses the potential to effectively manage exceedingly high levels of RF power. This anticipation is rooted in the observation that there are no apparent characteristics of LM that should inherently constrain its power handling capacity. The capability of the LM phase shifters to manage power is expected to be primarily bounded by the power handling limits of the SIW transmission line it employs, and this limit is notably substantial. Furthermore, the proposed LM phase shifter exhibits a significantly greater phase shift of 360°. This stands in contrast to the phase shifts of 180° for [32] and 67° for [51]. Moreover, when compared with [32], the suggested phase shifter presents a notably simpler design, requiring significantly fewer LM vias and occupying a considerably smaller footprint. Additionally, the proposed phase shifter boasts the capability of seamless integration within a phased array system, as exemplified in this paper. Conversely, the design outlined in [32] lacks suitability for integration within an SIW feeding structure. The phase shifter detailed in [32] features larger dimensions and relies on switching between distinct SIW transmission lines with varying electrical lengths to achieve phase shift. This methodology demands a substantial physical size to accommodate the divergent paths necessary for achieving the intended phase shift. However, the proposed phase shifter does have certain drawbacks, primarily in terms of resolution and physical size when compared to CMOS, GaN, Ferroelectric, and LC-based phase shifters. Notably, other phase shifters documented in [14], [15], [17], [18], [19], [20], [21], [22], [23], [24], [25], [26], and [64] offer significantly better resolution and are more compact in size than the proposed LM phase shifter. On the other hand, the alternative phase shifters in [14], [15], [16], [17], [18], [19], [20], [21], [22], [23], [24], [25], [26], and [64] exhibit inferior figures of merit (FoM) and insertion loss (IL) performance when compared to the proposed LM phase shifters. Additionally, these alternative phase shifters are also limited in their power handling capability, unlike the proposed LM phase shifters.

TABLE 3. The measured results of the proposed phase shifter at 10 GHz.

State	Number of active LM vias	Simulated total phase shift (phase step)	Measured total phase shift (phase step)	Measured IL (dB)
State 1 (S1)	0	NA	NA	1.7
State 2 (S2)	1	30.5° (30.5°)	31.2° (31.2°)	2.3
State 3 (S3)	2	77.8° (47.3°)	81.8° (50.6°)	1.9
State 4 (S4)	3	125.3° (47.5°)	132.3° (50.5°)	1.9
State 5 (S5)	4	172.7° (47.4°)	179° (46.7°)	2.0
State 6 (S6)	5	219.5° (46.8°)	223.8° (44.8°)	2.1
State 7 (S7)	6	267° (47.5°)	277.9° (53.1°)	2.7
State 8 (S8)	7	313.9° (46.9°)	323.4° (46.5°)	2.3
State 9 (S9)	8	360.5° (46.6°)	367.6° (44.2°)	2.8
	Total	360.5	367.6	

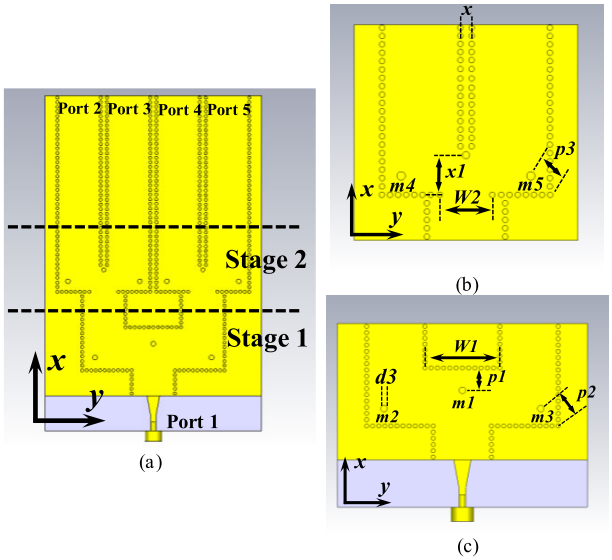

FIGURE 9. Schematic of the SIW power splitters incorporated within the phased array antenna. (a) Top view of the entire 1 × 4 power splitter, (b) 1 × 2 power splitter associated with Stage 2, (c) 1 × 2 power splitter associated with Stage 1 T-junction. [m1, m2, m3, m4, m5 stand for matching vias with diameter d3 = 1.6mm]. [W1=18mm, p1= 5.4mm, p2= 5.9mm, p3= 4.85mm, d3= 1.6mm, W2=9.4mm,x= 2mm, x1=7.1mm].

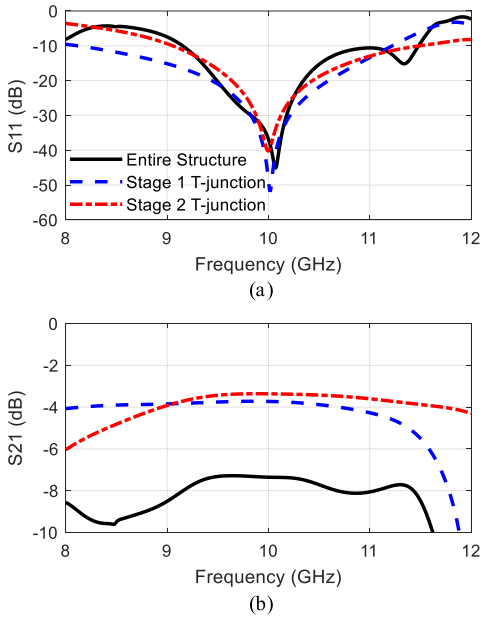

FIGURE 10. Simulated reflection coefficient (S11) and transmission coefficient (S21) of the entire 1 × 4 power splitter together with those of the 1 × 2 power splitters associated with stages 1 and 2. (a) S11 and (b) S21. [S31 performance is identical to S21 for both stage 1 and stage 2. Similarly, for the entire structure, S31, S41, S51 are all identical to S21].

IV. DESIGN CRITERION FOR THE LM PHASED ARRAY

A. DESIGN OF 1× 4 SIW POWER SPLITTER

Firstly, a 1 × 4 SIW power splitter was developed. Fig. 9(a) shows the configuration of the power splitter. The SIW feeding structure can be split into two stages. Each stage consists of 1 × 2 SIW power splitter. Fig. 9(c) shows the configuration of the first stage of the feeding structure. Fig. 9(b) shows the configuration of the second stage of the feeding structure Fig. 10 shows the performance of the entire 1 × 4 SIW power splitter together with that of the 1 × 2 power splitters associated with stages 1 and 2. Fig. 10 (a) shows the reflection coefficients (S_{11}) and Fig. 10(b) shows the transmission coefficient (S_{21}) of the entire 1 × 4 SIW power splitter together with that of the 1 × 2 power splitters associated with stages 1 and 2. All structures are designed to have a good impedance match together with a low *IL* at the centre frequency of 10GHz. The entire 1 × 4 SIW power splitters has a 10dB return loss bandwdith of 2.6 GHz ranging from 9.15GHz to 11.45GHz. For example at 10GHz the simulated IL of the 1 × 2 SIW power splitter associated with stage 1 is 3.7 dB and he IL of the 1 × 2 SIW power splitter associated with stage 2 is 3.38 dB. The IL of the entire 1 × 4 SIW power splitter is better than 7.36dB over a 1GHz bandwidth ranging from 9.5GHz to 10.5 GHz, while the IL is better than 8 dB over the 2.6GHz from 9.15 GHz to 11.45 GHz. Accoding to simulation the total losses within the 1-to-4 feeding structure is 7.36dB at 10GHz. Given that an ideal 1-to-4 feed has a splitting loss of 6dB. We can conclude that 1.36dB is caused by matching, SMA connector and dissipation losses within the substrate material.

B. PROTOTYPE FOR THE ENTIRE PHASED ARRAY INCORPORATING PRINTED DIPOLE RADIATORS

The next stage in the process of designing the phased array antenna is to integrate the four LM phase shifters within the 1 × 4 SIW power splitter and add 4 printed dipole antennas, as shown in Fig. 11(a). The printed dipole antenna array consists of four radiating elements. Each element resonates at 10 GHz with a 10 dB return loss impedance bandwidth of 1.5 GHz ranging from 9.2 GHz to 10.7GHz, as shown in Fig. 11(b). The radiating element was designed, based on the principles discussed in [66], [67], and [68], to resonate and achieve peak directivity at 10GHz. The resonant frequency of the dipole is controlled by the length of the dipole *DL* and the depth of resonance (i.e. matching at the resonant frequency) is controlled by *AL*. The physical spacing between each of the printed dipole elements, within the array, is *L2* =

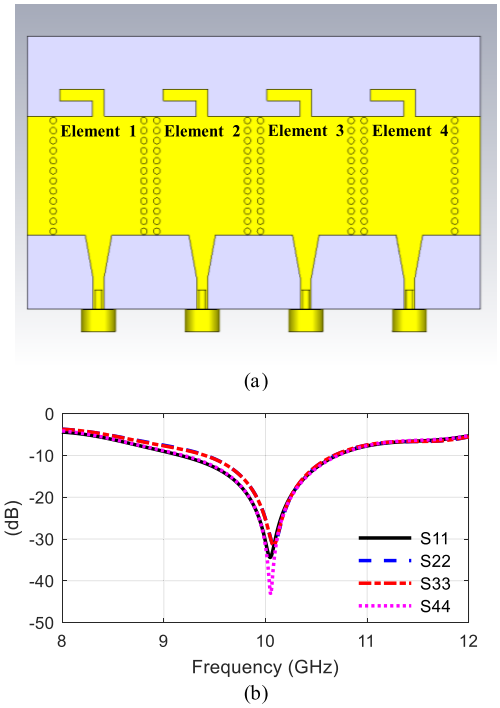

FIGURE 11. Schematic and the simulated reflection coefficients performance of the 1 × 4 element printed dipole array antenna. (a) Top view of the array and (b) reflection coefficients for each individual element.

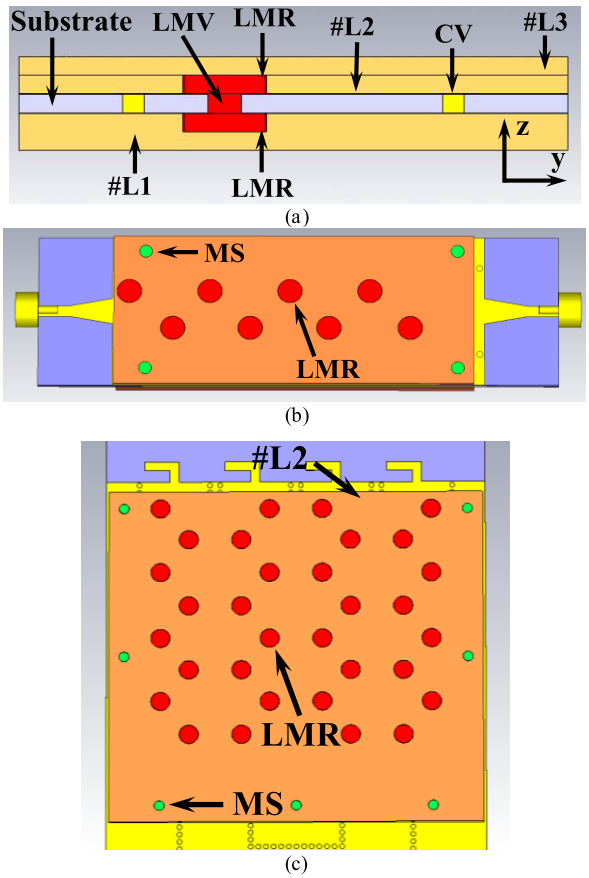

FIGURE 12. The entire phased array incorporating printed dipole elements and a Perspex cover above the LM channels. (a) cross section view in the z-y plane, (b), and (c) top view. Key: MS = Metallic screw, #L1 = Perspex Layer 1, #L2 = Perspex layer 2, #L3 = Perspex layer 3, LMR = Liquid metal reservoir, LMV = Liquid metal via, CV = Copper via. Metallic screw = green, Substrate = purple, Perspex = Orange, Copper plated vias = yellow, Liquid metal vias = red.

16 mm which corresponds to 0.53λ; where λ is the free-space operation wavelength at 10GHz. The isolation between any two adjacent elements in the antenna array is less than 14 dB. The peak simulated gain of each of Elements 1 to Element 4 is: 4.9dBi, 3.9dBi, 3.9dBi and 5.4dBi, respectively. Element 2 and Element 3 has lower gain performance than Elements 1 and 4 due to the increased mutual coupling between neighboring elements. Furthermore, Element 1 has a simulated side lobe level (SLL) of 9.2dB, element 2 has a SLL of 8.3dB, element 3 has a SLL of 8.3dB and element 4 has a SLL of 9.3dB. The simulated total efficiency at 10 GHz is higher than 90% for Elements 1 and 4 and higher than 85% for Element 2 and 3.

V. FABRICATION CONSIDERATION

This section of the paper discusses the fabrication of the hardware prototype, shown in Figs. 1 and 2. It also discusses the actuation of liquid metal (LM). The hardware prototype was fabricated and actuated as shown in Fig. 12. The structure responsible for confining and guiding the liquid metal consists of a three layers arrangement using transparent Perspex material. In Fig. 12(a), these layers are designated as layer 1 (#L1), layer 2 (#L2), and layer 3 (#L3). Within this setup, layers 1 (#L1) and 2 (#L2) serve as reservoirs to contain the liquid metal (LMRs), while layer 3 (#L3) functions as a protective cover. External to the SIW, multiple metallic screws (MS) are positioned to secure the distinct Perspex layers together, as depicted in Fig. 12(b) and Fig. 12(c). Importantly, these screws exert no influence on the RF performance of the proposed phase shifters and the associated phased array. This lack of influence stems from the screws being situated outside the SIW structure. LM is introduced into and extracted from the drilled holes through the utilization of a syringe. This method of actuation is widely employed and has been documented in numerous studies, such as those in [33], [34], [35], [36], [37], [38], [39], [40], [41], [42], and [69]. Several alternative actuation techniques are also present in the literature, including: a) utilizing a micropump, as reported in [43], [44], [45], [46], and [47], and b) employing electrochemically controlled capillary action, as explained in [48] and [49]. It is worth noting that any of these techniques could potentially be adopted to actuate the proposed devices in this paper. Importantly, altering the actuation approach will not cause any impact on the RF performance of either the phased array or the phase shifters. This is due to the feasibility of situating the actuation circuits either above or below the ground plane of the SIW feeding structure in the phased array. Moreover, these circuits can be

positioned far removed from the radiating elements, where the intensity of the electric field (E-field) and magnetic field (H-field) are exceptionally low.

The chosen via size (via diameter, d) is set at 1.8 mm to enable a smooth and repeatable process of filling the holes with liquid metal (LM), minimizing any associated issues. Based on our experience, filling vias with LM becomes technically challenging if their diameter is below 0.9 mm. Conversely, vias with diameters larger than 0.9 mm prove more manageable to fill. This is due to the fact that larger vias possess greater surface area; for instance, a via with a diameter of 1.8 mm boasts nearly four times the area of a 0.9 mm diameter via. Interestingly, simulation findings indicate that the via size has a relatively limited impact on the RF performance of the phase shifter. Vias with diameters less than 2 mm remain electrically small at 10GHz, resulting in negligible radiation and power leakage. Consequently, a recommended via size falls between 1 mm and 2 mm for the intended application. The primary advantage of employing larger vias lies in the ease of filling them with LM. However, when the via diameter exceeds 2 mm, a notable *IL* emerges when the vias are devoid of LM. For example, increasing the via diameter to 3 mm introduces an additional *IL* of around 0.25 dB. Importantly, we observed that no LM residues remained after emptying the vias. In addition, we routinely employ the liquid metal multiple times to actuate both of the proposed devices, and our observations reveal that this repetitive usage has no discernible impact on the RF performance of either component. As for the reconfiguration time of the proposed phased array, it is projected to fall within the range of milliseconds to seconds, as detailed in [43] and [45]. This range is relatively slower compared to certain alternative devices. Notably, the literature reports LM actuation speeds of up to 30 cm/s [70], and it is reasonable to expect that further advancements could lead to even higher actuation speeds. The velocity of actuation hinges on the volume of liquid metal being injected. Given that the actuation of a via entails the movement of a minute volume of liquid metal (sub-μL), rapid speeds are anticipated.

VI. EXPERIMENTAL RESULTS OF LM PHASED ARRAY

This section of the paper presents the measured results and the numerical simulation results for the proposed LM phased antenna array. The array of printed dipoles produce a beam that can be steered in the x-y plane). The performance of the phased array was predicted through computer simulation in CST Microwave Studio. The phased array was tested in several states which provide beam steering up to a maximum scan angle of $\pm 38°$ in the x-y plane. Note that the electric field radiation pattern (E-field) is in the x-y plane, while the magnetic field radiation pattern (H-field) is in the x-z plane. The beam of the proposed phased array is switched in the x-y plane which is equivalent to beam scanning in a conventional phased array. Fig. 13 and TABLE 5 shows the simulated and measured radiation patterns for the proposed phased array in each of the seven steered angles considered (note that those

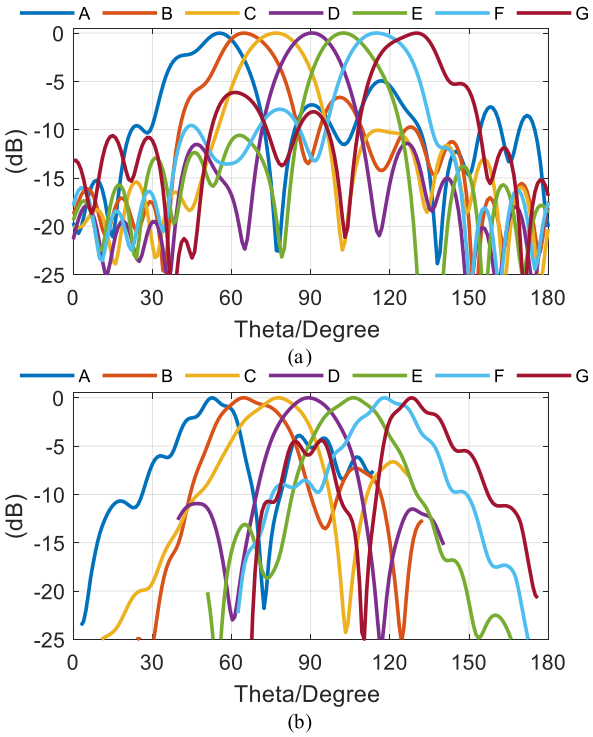

FIGURE 13. The normalized radiation patterns associated with the proposed phased array antenna at 10 GHz in the E-plane (x-y) plane. (a) Simulated result and (b) measured result.

angles are labeled case A to G). The figure shows radiating patterns at 10GHz. There is very good agreement between the simulated and measured radiation pattern and beam steering angle as shown in TABLE. 5. Measurements results show that the main beam of the proposed phased array antenna can be scanned, in the x-y plane within range of $\pm 38°$. TABLE 6 summarises the phase difference between the phase shifts provided by the four LM phase shifter in order to steer the beam towards a certain angle. In case D: the phased array radiates in the end-fire direction with no beam steering i.e. towards (91°). The difference in phase between the LM phase shifters is 0°. In cases C and E: the phase difference between consecutive LM phase shifter is $\pm 45°$, respectively. While in cases B and F the phase difference between consecutive LM phase shifter is $\pm 90°$, respectively. Finally, in cases A and G, the phase difference between consecutive LM phase shifters is $\pm 135°$, respectively.

Good agreement is observed between the measured and simulated S_{11} performance, as shown in Fig. 14. In all cases, the measured 10dB return loss bandwidth of the phased array is wider than 1GHz. In addition, the phased array provides beam steering over this entire bandwidth. Fig. 15 plots the measured gain as a function of frequency along with the measured side lobe level (SLL) and scan loss as a function of steered angle.

At 10 GHz the proposed phased array exhibits a measured gain of 8.3dBi which is 0.8dB less than the simulated gain at the same frequency. The peak value of measured gain

TABLE 4. Performance comparison between the proposed Liquid metal phase shifter and other alternative phase shifters.

Reference	Technology	Frequency (GHz)	Phase shifting Range (°) ($\emptyset_{max}$)	IL (dB)	FoM (°/dB)	Resolution (°)	RMS phase error (°)	RMS amplitude error (dB)	Size (mm)
This work	Liquid Metal	10	367.6	<2.8	131.3	≈45	20	<1.5	57.2 × 14
[32]	Liquid Metal	10	180	2.3	78.3	10	10	NA	87.2 × 56.2
[51]	Liquid Metal	5.6	≈67	≈1	70	NA	NA	NA	NA
[14]	Ferroelectric based	10	342	<8	52	NA	8.5	>2.5	2.8 × 3
[15]	Ferroelectric based	10	413	10.3	40.1	NA	NA	>3	3.8 × 2.3
[16]	Ferrite - LTCC	10.6	215	<7	48	NA	NA	NA	≈45 × 45
[17]	Liquid Crystal	10	≈60	≈2.5	≈24	NA	NA	NA	NA
[18]	Liquid Crystal	10	≈101	≈5	≈15.2	NA	NA	NA	NA
[19]	Liquid Crystal	10	≈100	≈3.9	NA	NA	NA	>3	< 4 × 1
[20]	5 bit MEMS	10	360	≈6	≈60	11	<10	>4	≈9 × 1.2
[22]	GaN	10	180	14	12.8	11.25	4.5	≈0.6	4.7 × 5
[23]	GaN	10	22.5 or 45	<5	≈11	NA	≈5.6	1.1	≈1 × 1
[24]	0.25 μm SiGe BiCMOS	10	360	> 12	< 30	11.25	6.4	>3.0	1.87× 0.88
[64]	0.13μm CMOS	10	360	13.2	27.3	5.625	4.1	≈0.8	2.06 × 0.58
[25]	0.18μm SiGe BiCMOS	10	≈348	≈8	≈43.5	11.25	4.6	0.6	NA
[26]	0.25μm SiGe BiCMOS	10	≈360	≈13	≈27.7	5.6	4	0.6	0.94 × 3.42
[65]	PIN Diode - SIW	10	<180	≈2	≈90	NA	NA	>0.8	NA

TABLE 5. Phased array beam switching in the x-z plane.

Case	Phase difference between phase shifters	Simulated Beam Direction	Measured Beam Direction
A	135°	55°	52°
B	90°	65°	64°
C	45°	77°	78°
D	0°	91°	89°
E	−45°	102°	106°
F	−90°	115°	117°
G	−135°	130°	128°

TABLE 6. Phased shifters configuration in the Phased array antenna.

State	Phase State (Phase shifter 1)	Phase State (Phase shifter 2)	Phase State (Phase shifter 3)	Phase State (Phase shifter 4)
A	S4 (≈ 135°)	S6 (≈ 270°)	S2 (≈ 45°)	S5 (≈ 180°)
B	S3 (≈ 90 °)	S5 (≈ 180°)	S7 (≈ 270°)	S9 (≈ 360°)
C	S2 (≈ 45°)	S3 (≈ 90°)	S4 (≈ 135°)	S5 (≈ 180°)
D	S1 (0°)	S1 (0°)	S1 (0°)	S1 (0°)
E	S5 (≈ 180°)	S4 (≈ 135°)	S3 (≈ 90°)	S2 (≈ 45°)
F	S9 (≈ 360°)	S7 (≈ 270°)	S5 (≈ 180°)	S3 (≈ 90°)
G	S5 (≈ 180°)	S2 (≈ 45°)	S7 (≈ 270°)	S4 (≈ 135°)

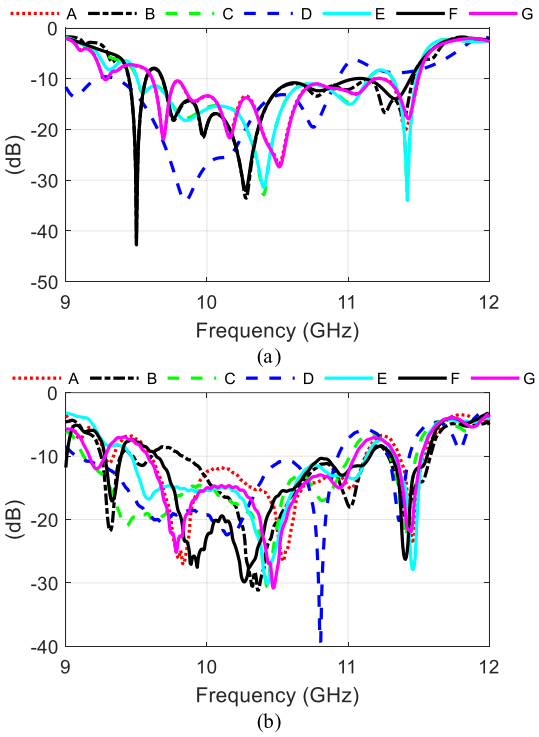

FIGURE 14. Reflection coefficient (S_{11}) of the LM phased array antenna in all states. (a) Simulated result and (b) measured result.

occurs at 10.2GHz and is 8.5dBi. This is 0.6dB less than the simulated gain at the same frequency. Overall, the measured gain of the proposed phased array remains higher than 7.9 dBi over a bandwidth greater than 1GHz, ranging from 9.6 GHz to 10.8GHz. In addition, the minor discrepancies observed between the gain of the proposed phased array antenna depicted in Figure 15(a) from the simulated and measured results can be mainly attributed to errors that arise during the manufacturing process of the PCB. It should be noted that the difference between the simulated and measured gain of the array falls within the range of 0.2dB to 0.8dB across a bandwidth of 1.5GHz, spanning from 9.5GHz to 11GHz. This difference can be attributed to the tolerances in fabrication that pertain to the position of LM vias, the dimensions of the feeding networks and the dipole antenna, as well as the dimensions of the microstrip to SIW transition. Good agreement is observed between the simulated and the

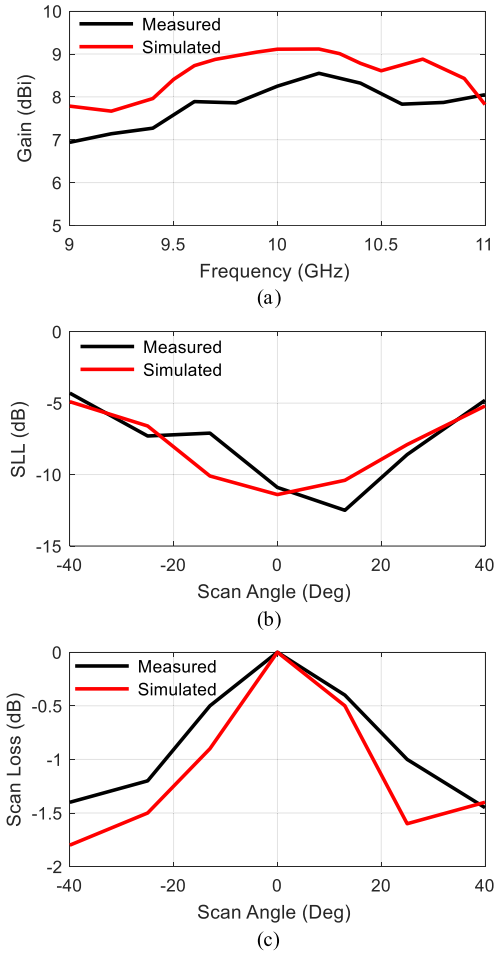

FIGURE 15. Gain, side love level (SLL) and scan loss performance. (a) Gain, (b) SLL at 10 GHz, and (c) scan loss at 10 GHz.

measured SLL performance for all of the seven steered angles considered (note that they are labeled case A to G). Fig. 15(b) shows that the proposed phased array has a measured SLL of −11.1dB in case D, −12.5dB in case E, −8.6 dB in case F and −4.9 dB in case G. In addition, the measured SLL is −7.1dB in case C, −7.3dB in case B and −4.5dB in case A. However, the proposed phased array antenna is suitable for application where high RF power handling capability is required. In the future, the SLL performance of the phased array can be improved by integrating an antenna element that have lower SLL than the proposed dipole antennas that radiate in the endfire direction or with antenna elements that radiate in the boresight direction. For example, a slot array antenna that radiate in the boresight direction and capable of delivering high gain and low SLL in similar manner to designs in [71], [72], [73], [74], [75], and [76] can be integrated with the proposed SIW feeding structure and LM phase shifters. Fig. 15(c) shows that the measured scan loss is less than −0.5dB in cases C and D. Furthermore, the scan loss is −1dB in case F and −1.2dB in case B, while it drops to 1.4dB and 1.5dB in cases G and A, respectively.

VII. CONCLUSION

This paper introduced the first experiment proof of using liquid metals to perform a wide range of phase control to design SIW phased antenna array. The proposed phased array antenna is based around SIW which is used to excite 1 × 4 printed dipole antenna array. The proposed LM phased array is a cost effective solution which offers low loss and wideband performance over the existing technology.

Novel LM based phase shifters are integrated with the SIW power dividers to effectively control the phase distribution inside the SIW. This provides a large-phase tuning ratio of 360°. Four LM phase shifters are integrated with the SIW feeding structure to realize the proposed phased array. Each phase shifter incorporates 8 LM vias and thus the total phase shift is divided into 8 steps of ∼45° each. Reconfiguration between the different phase states is achieved by adding/removing LM vias. Each phase shifter incorporates a total of eight LM vias.

Measured and simulated results, provided in the paper, serve to demonstrate that the performance of the proposed phased array antenna is excellent. The proposed phased array antenna operates on 10 GHz with the scanning range of ±38° along the end-fire direction with an impedance bandwidth wider than 10% and peak gain of 8.3 dBi. Finally, the proposed phase array antennas is an innovative solution offers various important advantages over the existing technology, including: low insertion loss (IL) and wideband performance with the potential for very high power handling capability.

ACKNOWLEDGMENT

The authors would like to thank Rogers Corporation who donated substrates used in the prototypes.

REFERENCES

[1] D. Parker and D. C. Zimmermann, "Phased arrays—Part 1: Theory and architectures," *IEEE Trans. Microw. Theory Techn.*, vol. 50, no. 3, pp. 678–687, Mar. 2002.

[2] D. Parker and D. C. Zimmermann, "Phased arrays—Part II: Implementations, applications, and future trends," *IEEE Trans. Microw. Theory Techn.*, vol. 50, no. 3, pp. 688–698, Mar. 2002.

[3] J. Ha, M. A. Elmansouri, and D. S. Filipovic, "A compact ultrawideband reflector antenna: Using a wide-band omnidirectional antenna with a mechanically steerable endfire beam to illuminate a half-cut paraboloid reflector," *IEEE Antennas Propag. Mag.*, vol. 60, no. 3, pp. 75–86, Jun. 2018.

[4] Y. Sun, F. Dang, C. Yuan, J. He, Q. Zhang, and X. Zhao, "A beam-steerable lens antenna for Ku-band high-power microwave applications," *IEEE Trans. Antennas Propag.*, vol. 68, no. 11, pp. 7580–7583, Nov. 2020.

[5] D. Sievenpiper, J. Schaffner, J. J. Lee, and S. Livingston, "A steerable leaky-wave antenna using a tunable impedance ground plane," *IEEE Antennas Wireless Propag. Lett.*, vol. 1, pp. 179–182, 2002.

[6] M. S. Rabbani, J. Churm, and A. Feresidis, "Electro-mechanically tunable meta-surfaces for beam-steered antennas from mm-wave to THz," in *Proc. 14th Eur. Conf. Antennas Propag. (EuCAP)*, Mar. 2020, pp. 1–4.

[7] P. Sanchez-Olivares, J. L. Masa-Campos, A. T. Muriel-Barrado, R. Villena-Medina, and G. M. Fernandez-Romero, "Mechanically reconfigurable linear array antenna fed by a tunable corporate waveguide network with tuning screws," *IEEE Antennas Wireless Propag. Lett.*, vol. 17, no. 8, pp. 1430–1434, Aug. 2018.

[8] H. L. Zhu, X. H. Liu, S. W. Cheung, and T. I. Yuk, "Frequency-reconfigurable antenna using metasurface," *IEEE Trans. Antennas Propag.*, vol. 62, no. 1, pp. 80–85, Jan. 2014.

[9] R. Guzmán-Quirós, A. R. Weily, J. L. Gómez-Tornero, and Y. J. Guo, "A Fabry–Pérot antenna with two-dimensional electronic beam scanning," *IEEE Trans. Antennas Propag.*, vol. 64, no. 4, pp. 1536–1541, Apr. 2016.

[10] D. F. Sievenpiper, J. H. Schaffner, H. J. Song, R. Y. Loo, and G. Tangonan, "Two-dimensional beam steering using an electrically tunable impedance surface," *IEEE Trans. Antennas Propag.*, vol. 51, no. 10, pp. 2713–2722, Oct. 2003.

[11] P. Deo, A. Mehta, D. Mirshekar-Syahkal, P. J. Massey, and H. Nakano, "Thickness reduction and performance enhancement of steerable square loop antenna using hybrid high impedance surface," *IEEE Trans. Antennas Propag.*, vol. 58, no. 5, pp. 1477–1485, May 2010.

[12] H. Zhou, A. Pal, A. Mehta, D. Mirshekar-Syahkal, and H. Nakano, "A four-arm circularly polarized high-gain high-tilt beam curl antenna for beam steering applications," *IEEE Antennas Wireless Propag. Lett.*, vol. 17, no. 6, pp. 1034–1038, Jun. 2018.

[13] X. Miao, W. Wan, Z. Duan, and W. Geyi, "Design of dual-mode arc-shaped dipole arrays for indoor base-station applications," *IEEE Antennas Wireless Propag. Lett.*, vol. 18, no. 4, pp. 752–756, Apr. 2019.

[14] M. Sazegar, Y. Zheng, H. Maune, C. Damm, X. Zhou, J. Binder, and R. Jakoby, "Low-cost phased-array antenna using compact tunable phase shifters based on ferroelectric ceramics," *IEEE Trans. Microw. Theory Techn.*, vol. 59, no. 5, pp. 1265–1273, May 2011.

[15] M. Sazegar, Y. Zheng, H. Maune, C. Damm, X. Zhou, and R. Jakoby, "Compact tunable phase shifters on screen-printed BST for balanced phased arrays," *IEEE Trans. Microw. Theory Techn.*, vol. 59, no. 12, pp. 3331–3337, Dec. 2011.

[16] S. Kagita, A. Basu, and S. K. Koul, "Characterization of LTCC-based ferrite tape in *X*-band and its application to electrically tunable phase shifter and notch filter," *IEEE Trans. Magn.*, vol. 53, no. 1, pp. 1–8, Jan. 2017.

[17] D. Wang, E. Polat, H. Tesmer, R. Jakoby, and H. Maune, "Highly miniaturized continuously tunable phase shifter based on liquid crystal and defected ground structures," *IEEE Microw. Wireless Compon. Lett.*, vol. 32, no. 6, pp. 519–522, Jun. 2022, doi: 10.1109/LMWC.2022.3142410.

[18] C. Ding, F.-Y. Meng, J.-Q. Han, H.-L. Mu, Q.-Y. Fang, and Q. Wu, "Design of filtering tunable liquid crystal phase shifter based on spoof surface plasmon polaritons in PCB technology," *IEEE Trans. Compon., Packag., Manuf. Technol.*, vol. 9, no. 12, pp. 2418–2426, Dec. 2019.

[19] A.-L. Franc, O. H. Karabey, G. Rehder, E. Pistono, R. Jakoby, and P. Ferrari, "Compact and broadband millimeter-wave electrically tunable phase shifter combining slow-wave effect with liquid crystal technology," *IEEE Trans. Microw. Theory Techn.*, vol. 61, no. 11, pp. 3905–3915, Nov. 2013.

[20] M. A. Morton and J. Papapolymerou, "A packaged MEMS-based 5-bit *X*-band high-pass/low-pass phase shifter," *IEEE Trans. Microw. Theory Techn.*, vol. 56, no. 9, pp. 2025–2031, Sep. 2008.

[21] M. Teshiba, R. Van Leeuwen, G. Sakamoto, and T. Cisco, "A SiGe MMIC 6-bit PIN diode phase shifter," *IEEE Microw. Wireless Compon. Lett.*, vol. 12, no. 12, pp. 500–501, Dec. 2002.

[22] W. Luo, H. Liu, Z. Zhang, P. Sun, and X. Liu, "High-power *X*-band 5-b GaN phase shifter with monolithic integrated E/D HEMTs control logic," *IEEE Trans. Electron Devices*, vol. 64, no. 9, pp. 3627–3633, Sep. 2017.

[23] T. N. Ross, K. Hettak, G. Cormier, and J. S. Wight, "Design of X-band GaN phase shifters," *IEEE Trans. Microw. Theory Techn.*, vol. 63, no. 1, pp. 244–255, Jan. 2015.

[24] B. Cetindogan, E. Ozeren, B. Ustundag, M. Kaynak, and Y. Gurbuz, "A 6 bit vector-sum phase shifter with a decoder based control circuit for X-band phased-arrays," *IEEE Microw. Wireless Compon. Lett.*, vol. 26, no. 1, pp. 64–66, Jan. 2016.

[25] Z. Li, J. Qiao, and Y. Zhuang, "An X-band 5-bit active phase shifter based on a novel vector-sum technique in 0.18μm SiGe BiCMOS," *IEEE Trans. Circuits Syst. II, Exp. Briefs*, vol. 68, no. 6, pp. 1763–1767, Jun. 2021.

[26] A. Burak, C. Çaliskan, M. Yazici, and Y. Gurbuz, "X-band 6-bit SiGe BiCMOS multifunctional chip with +12 dBm IP1dB and flat-gain response," *IEEE Trans. Circuits Syst. II, Exp. Briefs*, vol. 68, no. 1, pp. 126–130, Jan. 2021.

[27] M. Sayginer and G. M. Rebeiz, "An eight-element 2–16-GHz programmable phased array receiver with one, two, or four simultaneous beams in SiGe BiCMOS," *IEEE Trans. Microw. Theory Techn.*, vol. 64, no. 12, pp. 4585–4597, Dec. 2016.

[28] S. Alkaraki, A. L. Borja, J. Kelly, S. F. Jilani, R. Mittra, and Y. Gao, "Phase reconfiguration via SIW structures filled with liquid metal," in *Proc. 16th Eur. Conf. Antennas Propag. (EuCAP)*, Mar. 2022, pp. 1–5.

[29] S. Khan, N. Vahabisani, and M. Daneshmand, "A fully 3-D printed waveguide and its application as microfluidically controlled waveguide switch," *IEEE Trans. Compon., Packag., Manuf. Technol.*, vol. 7, no. 1, pp. 70–80, Jan. 2017.

[30] N. Vahabisani, S. Khan, and M. Daneshmand, "A K-band reflective waveguide switch using liquid metal," *IEEE Antennas Wireless Propag. Lett.*, vol. 16, pp. 1788–1791, 2017.

[31] S. Alkaraki, J. Kelly, A. L. Borja, R. Mittra, and Y. Wang, "Gallium-based liquid metal substrate integrated waveguide switches," *IEEE Microw. Wireless Compon. Lett.*, vol. 31, no. 3, pp. 257–260, Mar. 2021.

[32] S. Alkaraki, A. L. Borja, J. R. Kelly, R. Mittra, and Y. Gao, "Reconfigurable liquid metal-based SIW phase shifter," *IEEE Trans. Microw. Theory Techn.*, vol. 70, no. 1, pp. 323–333, Jan. 2022.

[33] A. M. Morishita, C. K. Y. Kitamura, A. T. Ohta, and W. A. Shiroma, "A liquid-metal monopole array with tunable frequency, gain, and beam steering," *IEEE Antennas Wireless Propag. Lett.*, vol. 12, pp. 1388–1391, 2013.

[34] C. Wang, J. C. Yeo, H. Chu, C. T. Lim, and Y.-X. Guo, "Design of a reconfigurable patch antenna using the movement of liquid metal," *IEEE Antennas Wireless Propag. Lett.*, vol. 17, no. 6, pp. 974–977, Jun. 2018.

[35] W. Chen, Y. Li, R. Li, A. V. Thean, and Y.-X. Guo, "Bendable and stretchable microfluidic liquid metal-based filter," *IEEE Microw. Wireless Compon. Lett.*, vol. 28, no. 3, pp. 203–205, Mar. 2018.

[36] C. Koo, B. E. LeBlanc, M. Kelley, H. E. Fitzgerald, G. H. Huff, and A. Han, "Manipulating liquid metal droplets in microfluidic channels with minimized skin residues toward tunable RF applications," *J. Microelectromech. Syst.*, vol. 24, no. 4, pp. 1069–1076, Aug. 2015.

[37] M. A. Rafi, B. D. Wiltshire, and M. H. Zarifi, "Wideband tunable modified split ring resonator structure using liquid metal and 3-D printing," *IEEE Microw. Wireless Compon. Lett.*, vol. 30, no. 5, pp. 469–472, May 2020.

[38] A. Ha and K. Kim, "Frequency tunable liquid metal planar inverted-F antenna," *Electron. Lett.*, vol. 52, no. 2, pp. 100–102, Jan. 2016.

[39] A. M. Watson, T. F. Leary, K. S. Elassy, A. G. Mattamana, M. A. Rahman, W. A. Shiroma, A. T. Ohta, and C. E. Tabor, "Physically reconfigurable RF liquid electronics via Laplace barriers," *IEEE Trans. Microw. Theory Techn.*, vol. 67, no. 12, pp. 4881–4889, Dec. 2019.

[40] L. Song, W. Gao, C. O. Chui, and Y. Rahmat-Samii, "Wideband frequency reconfigurable patch antenna with switchable slots based on liquid metal and 3-D printed microfluidics," *IEEE Trans. Antennas Propag.*, vol. 67, no. 5, pp. 2886–2895, May 2019.

[41] J.-H. Low, P.-S. Chee, and E.-H. Lim, "Deformable liquid metal patch antenna for air pressure detection," *IEEE Sensors J.*, vol. 20, no. 8, pp. 3963–3970, Apr. 2020.

[42] V. T. Bharambe, J. Ma, M. D. Dickey, and J. J. Adams, "Planar, multifunctional 3D printed antennas using liquid metal parasitics," *IEEE Access*, vol. 7, pp. 134245–134255, 2019.

[43] A. Qaroot and G. Mumcu, "Microfluidically reconfigurable reflection phase shifter," *IEEE Microw. Wireless Compon. Lett.*, vol. 28, no. 8, pp. 684–686, Aug. 2018.

[44] S. N. McClung, S. Saeedi, and H. H. Sigmarsson, "Band-reconfigurable filter with liquid metal actuation," *IEEE Trans. Microw. Theory Techn.*, vol. 66, no. 6, pp. 3073–3080, Jun. 2018.

[45] A. Dey and G. Mumcu, "Microfluidically controlled frequency-tunable monopole antenna for high-power applications," *IEEE Antennas Wireless Propag. Lett.*, vol. 15, pp. 226–229, 2016.

[46] D. Rodrigo, L. Jofre, and B. A. Cetiner, "Circular beam-steering reconfigurable antenna with liquid metal parasitics," *IEEE Trans. Antennas Propag.*, vol. 60, no. 4, pp. 1796–1802, Apr. 2012.

[47] S. Singh, J. Taylor, H. Zhou, A. Pal, A. Mehta, H. Nakano, and P. Howland, "A pattern and polarization reconfigurable liquid metal helical antenna," in *Proc. IEEE Int. Symp. Antennas Propag. USNC/URSI Nat. Radio Sci. Meeting*, Jul. 2018, pp. 857–858.

[48] M. Wang, C. Trlica, M. R. Khan, M. D. Dickey, and J. J. Adams, "A reconfigurable liquid metal antenna driven by electrochemically controlled capillarity," *J. Appl. Phys.*, vol. 117, no. 19, May 2015, Art. no. 194901.

[49] M. Wang, M. R. Khan, C. Trlica, M. D. Dickey, and J. J. Adams, "Pump-free feedback control of a frequency reconfigurable liquid metal monopole," in *Proc. IEEE Int. Symp. Antennas Propag. USNC/URSI Nat. Radio Sci. Meeting*, Jul. 2015, pp. 2223–2224.

[50] S. Alkaraki, J. Kelly, and Z. Wang, "Reconfigurable antenna using liquid metal vias," in *Proc. IEEE Int. Symp. Antennas Propag. USNC-URSI Radio Sci. Meeting (APS/URSI)*, Dec. 2021, pp. 315–316.

[51] J. H. Dang, R. C. Gough, A. M. Morishita, A. T. Ohta, and W. A. Shiroma, "Liquid-metal-based phase shifter with reconfigurable EBG filling factor," in *IEEE MTT-S Int. Microw. Symp. Dig.*, May 2015, pp. 1–4.

[52] S. Alkaraki, Z. Qu, J. Kelly, A. L. Borja, R. Mittra, and Y. Wang, "Liquid metal enabled SIW Vias and RF blocking walls for reconfigurable antennas," in *Proc. 16th Eur. Conf. Antennas Propag. (EuCAP)*, Mar. 2022, pp. 1–5.

[53] M. Wang, I. M. Kilgore, M. B. Steer, and J. J. Adams, "Characterization of intermodulation distortion in reconfigurable liquid metal antennas," *IEEE Antennas Wireless Propag. Lett.*, vol. 17, no. 2, pp. 279–282, Feb. 2018.

[54] K. Sellal, L. Talbi, T. A. Denidni, and J. Lebel, "Design and implementation of substrate integrated waveguide phase shifter," *IET Microw., Antennas Propag.*, vol. 2, pp. 194–197, Mar. 2008.

[55] K. Hettak, G. A. Morin, and M. G. Stubbs, "A novel miniature CPW topology of a high-pass/low-pass T-network phase shifter at 30 GHz," in *Proc. Eur. Microw. Conf. (EuMC)*, Oct. 2009, pp. 1140–1143.

[56] B. Koul and S. Bhat, *Microwave and Millimeter Wave Phase Shifters*, vol. 2 Norwood, MA, USA: Artech House, 1991, pp. 411–414.

[57] T. A. Abele, "Inductive post arrays in rectangular waveguide," *Bell Syst. Tech. J.*, vol. 57, no. 3, pp. 577–594, Mar. 1978.

[58] Y. Leviatan, P. G. Li, A. T. Adams, and J. Perini, "Single-post inductive obstacle in rectangular waveguide," *IEEE Trans. Microw. Theory Techn.*, vol. MTT-31, no. 10, pp. 806–812, Oct. 1983.

[59] N. Markuvitz, *Waveguide Handbook*. Exeter, U.K.: Short Run Press Ltd, 1986.

[60] L. Yan, W. Hong, K. Wu, and T. Cui, "Investigations on the propagation characteristics of the substrate integrated waveguide based on the method of lines," *IEE Proc. Microw. Antennas Propag.*, vol. 152, no. 1, pp. 35–42, Feb. 2005, doi: 10.1049/ip-map:20040726.

[61] J. E. Rayas-Sanchez and V. Gutierrez-Ayala, "A general EM-based design procedure for single-layer substrate integrated waveguide interconnects with microstrip transitions," in *IEEE MTT-S Int. Microw. Symp. Dig.*, Jun. 2008, pp. 983–986.

[62] F. Xu and K. Wu, "Guided-wave and leakage characteristics of substrate integrated waveguide," *IEEE Trans. Microw. Theory Techn.*, vol. 53, no. 1, pp. 66–73, Jan. 2005.

[63] D. Deslandes, "Design equations for tapered microstrip-to-substrate integrated waveguide transitions," in *IEEE MTT-S Int. Microw. Symp. Dig.*, May 2010, pp. 704–707.

[64] S. Sim, L. Jeon, and J.-G. Kim, "A compact X-band bi-directional phased-array T/R chipset in 0.13 μm CMOS technology," *IEEE Trans. Microw. Theory Techn.*, vol. 61, no. 1, pp. 562–569, Jan. 2013.

[65] B. Muneer, Z. Qi, and X. Shanjia, "A broadband tunable multilayer substrate integrated waveguide phase shifter," *IEEE Microw. Wireless Compon. Lett.*, vol. 25, no. 4, pp. 220–222, Apr. 2015.

[66] R. A. Alhalabi and G. M. Rebeiz, "High-gain Yagi–Uda antennas for millimeter-wave switched-beam systems," *IEEE Trans. Antennas Propag.*, vol. 57, no. 11, pp. 3672–3676, Nov. 2009.

[67] M. Ansari, H. Zhu, N. Shariati, and Y. J. Guo, "Compact planar beamforming array with endfire radiating elements for 5G applications," *IEEE Trans. Antennas Propag.*, vol. 67, no. 11, pp. 6859–6869, Nov. 2019.

[68] J. Zang, X. Wang, A. Alvarez-Melcon, and J. S. Gomez-Diaz, "Nonreciprocal Yagi–Uda filtering antennas," *IEEE Antennas Wireless Propag. Lett.*, vol. 18, no. 12, pp. 2661–2665, Dec. 2019.

[69] T. Kim, K. Kim, S. Kim, J. Lee, and W. Kim, "Micropatterning of liquid metal by dewetting," *J. Microelectromech. Syst.*, vol. 26, no. 6, pp. 1244–1247, Dec. 2017.

[70] M. R. Khan, C. Trlica, and M. D. Dickey, "Recapillarity: Electrochemically controlled capillary withdrawal of a liquid metal alloy from microchannels," *Adv. Funct. Mater.*, vol. 25, no. 5, pp. 671–678, Nov. 2014.

[71] H. Yang, G. Montisci, Z. Jin, Y. Liu, X. He, and G. Mazzarella, "Improved design of low sidelobe substrate integrated waveguide longitudinal slot array," *IEEE Antennas Wireless Propag. Lett.*, vol. 14, pp. 237–240, 2015.

[72] D.-J. Wei, J. Li, G. Yang, J. Liu, and J.-J. Yang, "Design of compact dual-band SIW slotted array antenna," *IEEE Antennas Wireless Propag. Lett.*, vol. 17, no. 6, pp. 1085–1089, Jun. 2018.

[73] C. Zhao, X. Li, C. Sun, H. Huang, and Y. Liu, "Design of a low-SLL SIW slot array antenna with a large declination in *Ka*-band," *IEEE Access*, vol. 7, pp. 120541–120547, 2019.

[74] S. E. Hosseininejad, N. Komjani, and A. Mohammadi, "Accurate design of planar slotted SIW array antennas," *IEEE Antennas Wireless Propag. Lett.*, vol. 14, pp. 261–264, 2015.

[75] Z. Ding, S. Xiao, M.-C. Tang, and C. Liu, "A compact highly efficient hybrid antenna array for W-band applications," *IEEE Antennas Wireless Propag. Lett.*, vol. 17, no. 8, pp. 1547–1551, Aug. 2018.

[76] L. Yan, W. Hong, G. Hua, J. Chen, K. Wu, and T. Jun Cui, "Simulation and experiment on SIW slot array antennas," *IEEE Microw. Wireless Compon. Lett.*, vol. 14, no. 9, pp. 446–448, Sep. 2004.

SHAKER ALKARAKI (Member, IEEE) received the B.Sc. degree (Hons.) in communication engineering from International Islamic University Malaysia (IIUM), Malaysia, Kuala Lumpur, Malaysia, in 2011, the M.Sc. degree (Hons.) from The University of Manchester (UoM), Manchester, U.K., in 2013, and the Ph.D. degree in electronic engineering from the Queen Mary University of London (QMUL), London, U.K., in 2019.

From June 2019 to March 2023, he was a Postdoctoral Researcher with the Antennas and Electromagnetics Group, QMUL. He is currently an Assistant Professor with the George Green Institute for Electromagnetics Research, Department of Electrical and Electronic Engineering, University of Nottingham, Nottingham, U.K. His research interests include interdisciplinary in nature and are in the intersection between antennas, microwave, millimeter-wave (mm-wave) engineering, wireless communication, 3D printing, material sciences, mm-wave and microwave-reconfigurable devices, mm-wave antennas and arrays, 3-D-printed antennas, 5G antennas and systems, multiple-input and multiple-output (MIMO) systems, leaky waves, liquid metal antennas, and microwave devices. He received the B.Sc. Scholarship from IIUM, the M.Sc. Scholarship from UoM, and the Ph.D. Scholarship from QMUL.

QUAN-WEI LIN (Member, IEEE) was born in Xinhui, Guangdong, China. He received the B.E. degree in information engineering and the M.E. degree in communication and information systems from the South China University of Technology, Guangzhou, China, in 2013 and 2016, respectively, and the Ph.D. degree in electrical engineering from the City University of Hong Kong, Hong Kong, in 2019. He joined the State Key Laboratory of Terahertz and Millimeter Waves, City University of Hong Kong, as a Postdoctoral Fellow, in 2019. His current research interests include millimeter-wave antennas, metasurfaces, and reconfigurable reflectarrays. He has published more than 30 international journals and conference papers. He was awarded four Chinese patents. He was a recipient of the Third Prize in the Student Innovation Competition of the 2013 IEEE International Workshop on Electromagnetics.

JAMES R. KELLY (Member, IEEE) was born in Derby, Derbyshire, U.K., in 1979. He received the master's degree in electronic and electrical engineering and the Ph.D. degree in microwave filters from Loughborough University, Loughborough, Leicestershire, U.K., in 2002 and 2007, respectively. From 1999 to 2000, he was with International Rail Vehicle Consultancy, Interfleet Technology. In 2001, he was a Trainee with the Rolls-Royce Strategic Research Centre. From 2007 to 2011, he was a Research Fellow/Associate with Loughborough University, and the Universities of Birmingham, and Sheffield. From 2011 until 2012, he was with Airbus Defence and Space Ltd. (then EADS Astrium). In 2012, he was a Research Associate with Durham University, U.K. In 2012, he joined Anglia Ruskin University, Cambridge, U.K., where he was a Lecturer. From 2013 to 2018, he was a Lecturer with the University of Surrey. He is currently a Senior Lecturer in reconfigurable microwave antennas with the School of Electronic Engineering and Computer Science, Queen Mary University of London (QMUL).

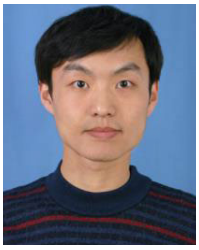

ZHENGPENG WANG (Member, IEEE) was born in Shandong, China, in 1981. He received the B.Sc. degree in electronic science and technology from Shandong University, Jinan, China, in 2004, and the M.Sc. and Ph.D. degrees in electromagnetic field and microwave technology from Beihang University, Beijing, China, in 2007 and 2012, respectively.

He was a Visiting Researcher with the Antenna and Applied Electromagnetic Laboratory, University of Birmingham, Birmingham, U.K., in 2009 and 2010. From 2013 to 2015, he was a Research Fellow with the University of Kent, Canterbury, U.K., and the University of Science and Technology Beijing, Beijing. He is currently an Associate Professor with Beihang University. His current research interests include over the air (OTA) test, reconfigurable antennas, compact antenna test range feed antenna, and antenna measurement.

HANG WONG (Senior Member, IEEE) received the B.Eng., M.Phil., and Ph.D. degrees in electronic engineering from the City University of Hong Kong (CityU), in 1999, 2002, and 2006, respectively. He joined the Department of Electrical Engineering, CityU, in 2012. He had several visiting professorships with Stanford University, USA; University of Waterloo, Canada; University of College London, U.K.; and University of Limoges, France, in 2011, 2013, 2014, and 2015 respectively. He is currently the Director of the Applied Electromagnetics Laboratory, CityU; and the Deputy Director of the State Key Laboratory of Terahertz and Millimeter Waves (Hong Kong). His research interests include the antenna technologies of 5G, 6G, millimeter-wave, and terahertz applications. His achievements led to receiving numerous awards at local, national, and international conferences. For example, he received the Best Paper Award at the National Conference 2017 Les Journées Nationales Microondes in France, the Best Paper Award at the 2017 IEEE International Workshop on Electromagnetics in the U.K., the Best Associate Editor Award 2016 of an IEEE Antennas and Wireless Propagation Letters in the USA, and the Outstanding Scientist Award of 2016 in Shenzhen city presented by Shenzhen Science and Technology Bureau. He was awarded to lead a major project supported by the Ministry of Industry and Information Technology of PRC to develop new antenna elements for TD-LTE and 5G applications. He has over 200 publications, two coauthors of book chapters, and 20 U.S. and Chinese patents. He is the Chair of the IEEE Hong Kong Section of the Antennas and Propagation (AP)/Microwave Theory and Techniques (MTT) Chapter. He is the IEEE APS Region-10 Representative. He was the General Co-Chair of the Asia Pacific Microwave Conference (AMPC) 2020, Hong Kong; and the General Chair of Cross-Strait Radio Science and Wireless Technology Conference 2021, Shenzhen, China. He is an Associate Editor of IEEE Transactions on Antennas and Propagation. He was the Associate Editor of IEEE Antennas and Wireless Propagation Letters.